ARTICLE

Check for updates

Phytoplankton abundance in the Barents Sea is predictable up to five years in advance

Filippa Fransner [1✉], Are Olsen [1], Marius Årthun [1], François Counillon [1,2], Jerry Tjiputra [3], Annette Samuelsen [2] & Noel Keenlyside [1,2]

The Barents Sea is a highly biologically productive Arctic shelf sea with several commercially important fish stocks. Interannual-to-decadal predictions of its ecosystem would therefore be valuable for marine resource management. Here, we demonstrate that the abundance of phytoplankton, the base of the marine food web, can be predicted up to five years in advance in the Barents Sea with the Norwegian Climate Prediction Model. We identify two different mechanisms giving rise to this predictability; 1) in the southern ice-free Atlantic Domain, skillful prediction is a result of the advection of waters with anomalous nitrate concentrations from the Subpolar North Atlantic; 2) in the northern Polar Domain, phytoplankton predictability is a result of the skillful prediction of the summer ice concentration, which influences the light availability. The skillful prediction of the phytoplankton abundance is an important step forward in the development of numerical ecosystem predictions of the Barents Sea.

---

[1] Geophysical Institute, University of Bergen, and Bjerknes Centre for Climate Research, Bergen, Norway. [2] Nansen Environmental and Remote Sensing Center, and Bjerknes Centre for Climate Research, Bergen, Norway. [3] NORCE Norwegian Research Centre, and Bjerknes Centre for Climate Research, Bergen, Norway. ✉email: filippa.fransner@uib.no

Hosting one of the World's largest cod-stocks[1], the Barents Sea fishery is of international importance. Reliable interannual-to-decadal predictions of the Barents Sea ecosystem would therefore be highly beneficial for society. The Barents Sea ecosystem, across all trophic levels, is strongly influenced by the inflow of Atlantic Water through the Barents Sea Opening[2–4] (Fig. 1). This warm and relatively saline water is brought to the Barents Sea from the Subpolar North Atlantic (SPNA) by the North- and Norwegian Atlantic currents with an advective lag of 2–10 years[3,5,6]. The heat that it carries exerts a strong influence on the temperature and sea ice extent in the Barents Sea[7–9] and thus shapes the environmental conditions for the organisms living there. Strong co-variability has, for example, been shown between phytoplankton activity and sea ice extent[6,10–13], where periods of low ice coverage are associated with higher productivity. Another seminal example is the relationship between ocean temperature and the size of the cod stock, in which larger cod-stocks are associated with warmer waters[2,3,14].

The thermal and dynamic memory residing in the Atlantic Water that is advected northward from the SPNA provides a potential for predicting the physical conditions of the Barents Sea several years ahead. With retro-perspective predictions, i.e., hindcasts, the winter sea ice cover has been shown to be predictable up to 2 years in advance with a statistical model based on the observed heat transport in the Barents Sea Opening[9]. Dynamical climate prediction models have successfully produced skillful predictions of the Barents Sea winter temperature from a few years up to a decade in advance[5,15], and it was demonstrated that the rapid decline in the winter Arctic sea ice extent in the Atlantic sector between 1997–2007 could be predicted 5–7 years in advance[16], in agreement with the advective time scale between the SPNA and the Barents Sea.

The long-term predictability of the Barents Sea's physical state, in combination with the physical-biological couplings mentioned above, give reason to believe that there is also a potential for predictions of the Barents Sea ecosystem. In fact, the Barents Sea cod stock has been shown to be predictable up to a decade in advance by the use of statistical models fed with upstream hydrographic anomalies[3,17]. However, no attempts have been made to predict the Barents Sea ecosystem dynamically using coupled physical-ecosystem numerical models. An important first step in this direction is successful predictions of phytoplankton primary production, the base of the marine food web. This requires skillful prediction of summer hydrography and sea ice, which is both challenging and little explored[18–24]. Here, we take this first step by using retrospective decadal hindcasts, produced with the Norwegian Climate Prediction Model (NorCPM1,[25]) in which primary production is simulated by the biogeochemical model HAMOCC[26]. The hindcasts have been initialized from a reanalysis into which observed temperature and salinity has been assimilated to bring the model as close as possible to the real state of the climate system. By comparing the hindcasts with satellite-derived chlorophyll and hydrographic measurements, we demonstrate that two specific events of high phytoplankton abundance can be predicted up to 5 years in advance in two distinct regions of the Barents Sea, and identify the mechanisms underlying this predictability.

Results and discussion
Prediction of phytoplankton abundance in NorCPM1. NorCPM1's skill to predict past interannual variability in phytoplankton concentration, as evident in the satellite record, shows a spatially varying pattern (Fig. 1). In the seasonally ice-covered region (from now on referred to as the Polar Domain), a significant positive correlation is found 2–9 years after the initialization of the hindcasts (i.e., in lead years 2–9). In the Atlantic Domain (defined as the region south of the maximum sea ice extent in Fig. 1b–d), however, NorCPM1 shows no predictive skill with this specific skill score. To get a better understanding of the drivers of the phytoplankton variations during the period of 1998–2018, and the mechanisms underlying the predictability, we analyze the time series of phytoplankton concentration, expressed in units of carbon, and potential physical and biogeochemical drivers in the next section. The Atlantic and Polar Domains are analyzed separately by extracting time series from the red and blue rectangles, respectively, in Fig. 1b–d. Due to the seasonality of phytoplankton dynamics, we focus on the early summer season, specifically the months of May–July, which covers the climatological peak concentration of phytoplankton in both the observations and model (thick lines in Supplementary Fig. S1a, b). Three-monthly means were chosen to minimize issues related to the lack of observational data and mismatch in the timing of the spring bloom.

Local drivers of phytoplankton predictability. In the Polar Domain, satellite observations show a positive anomaly in the phytoplankton abundance stretching over the 2000s and 2010s. The phytoplankton abundance increased, overall, between 2000 and 2010 (Fig. 2a). After this, the concentration has remained relatively stable. The reanalysis, which acts as a pseudo-observation[25,27], shows a similar behavior, showing that the assimilation of temperature and salinity also constrains the modeled phytoplankton dynamics. After removing the linear trend in the observed and modeled time series to exclude variability on longer time scales than resolved by our time series, the NorCPM1 hindcasts successfully predict the observed phytoplankton concentration up to lead year 5 (see also Supplementary Table S1 and Fig. S2). This means that the skill for longer lead years seen in Fig. 1 mainly comes from the linear trend in the time series. To verify that the predictive skill is not a result of external forcing, such as climate change, and that the predictability comes as a result of skillful initialization of the climate prediction model and its hindcasts, we analyze the evolution of the historical simulation. The historical simulation is an ensemble mean of 30 realizations that has been run under historical external forcing, including atmospheric greenhouse gasses, aerosols and solar radiation. The ensemble averaging eliminates the intrinsic climate variability, i.e., variability that arises from internal oceanic and atmospheric processes. The historical ensemble average is consequently a measure of the impact of the external forcing, including climate change, on the system. Between 2005 and 2014 (marked in blue shading), both the observations and the hindcasts show a similar evolution, which differs from the historical simulation. This indicates that a large part of the positive anomaly is a result of intrinsic climate variability, and that the predictability comes from skillful initialization of the hindcasts.

What caused this positive anomaly in phytoplankton concentration, and why was it predictable? Several studies have attributed the high Arctic primary production and phytoplankton abundance during this period of time to a drop in the sea ice extent[11,12,28,29], which increases the light availability and, thus, expands the area where phytoplankton can grow, as well as the length of their growing season. This pronounced drop in sea ice extent, associated with higher sea surface temperature and increased light availability, is also evident in our Polar Domain, both in satellite observations and the reanalysis, and is predicted in the hindcasts at lead year 5 (Fig. 2c, d, Supplementary Fig. S3a, and Table S1). The anomalously low sea ice concentration is not
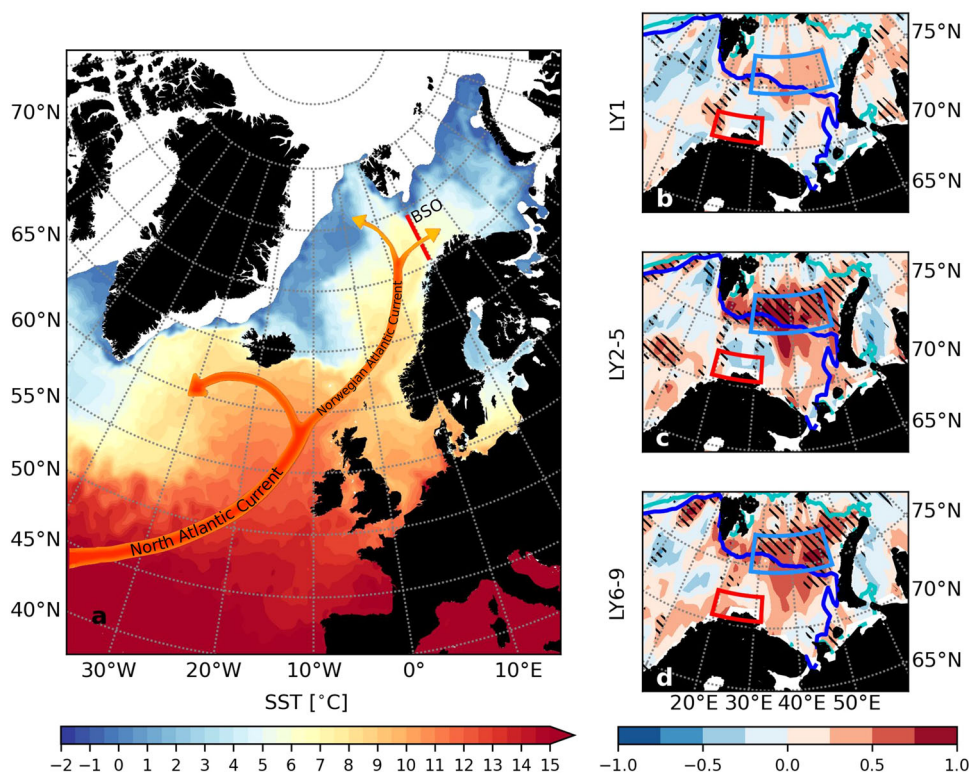
Fig. 1 Phytoplankton predictability. a Snapshot of SST in the Subpolar North Atlantic, and the Nordic and Barents seas from the OCCI dataset[67,68], daily mean from April 15 2007. Areas with an ice cover exceeding 30% are marked in white. The pathways of the North Atlantic and Norwegian Atlantic currents are marked with arrows. The Barents Sea Opening is marked with a red line. **b–d** Anomaly correlation (filled contours) between annual mean observed (satellite-derived) chlorophyll and dynamically predicted annual mean phytoplankton carbon concentration for the period of 1998–2018, for 1 year after the initialization (lead year 1) (**b**), lead years 2–5 (**c**), and lead years 6–9 (**d**). Striped regions indicate that the correlation is significantly different from zero and also significantly different from the correlation between the hindcasts and the historical simulation. The latter criterion ensures that the skill is associated with internal climate variability, and is not simply driven by external forcing (i.e., climate change). The blue and turquoise lines show the maximum (1998) and minimum (2006), respectively, summer (average over May–July) sea ice extent (30%) during the period 1998–2018.

seen in the historical simulation, corroborating that the event of high phytoplankton concentration and low sea ice extent was caused by climate variability. Associated with the negative anomaly in sea ice concentration, the reanalysis also shows a weakening of the vertical stratification and increased mixed layer depths (Supplementary Fig. S3c, d). This is a result of increasing surface salinity (not shown) that most likely follows the reduced input of meltwater in spring. A reduced vertical stratification increases the vertical mixing and can alleviate nutrient limitation, but can also increase the light limitation of the phytoplankton. However, the density difference anomaly that is predicted by the hindcasts at lead year 5 is not large enough to impact the mixed layer depth (Supplementary Fig. S3c and Table S1), and should, therefore, also have a negligible impact on the phytoplankton predictability.

In situ observations from the Polar Domain are very sparse, and mostly constrained to August and September. To exclude that the increasing phytoplankton abundance during 2005–2014 was co-driven by changes in nutrient availability at the start of the growing season, we resort to observations of deep (50–200 m) concentrations of nitrate and phosphate (Fig. 2b and Supplementary Fig. 3b). Since the water column is fully mixed in winter (the mean depth of the Barents Sea is only 230 m), these are expected to exhibit similar interannual and longer-term trends as the winter surface concentration (Fig. 2b). During 2005–2014, a negative anomaly is seen in the deep nutrient concentration both in the reanalysis and in the hindcasts at lead year 5, showing that the positive phytoplankton anomaly cannot be driven by increasing nutrients in the model. The in situ observations of nitrate and phosphate also indicate negative anomalies. These are more variable, however, but we do note that the variability is not much more than the typical accuracy of nitrate measurements, which is ~2%[30], compared to a mean deep nitrate concentration of 10 μmol l^{-1}.

In the Atlantic Domain, satellite observations show two peaks in chlorophyll concentration; one in the early 2000s and one in the early 2010s (Fig. 2e). The positive anomaly in the early 2000s is also evident in in situ chlorophyll observations, which are measured up to six times each year along the Fugløya-Bjørnøya section across the Barents Sea Opening, and in the reanalysis, confirming that this event is a robust feature. This specific event (marked in red shading in Fig. 2e) is skilfully predicted in the hindcasts in lead year 5 (see also Supplementary Fig. S4 and Table S2). Notably, the historical simulation does not show any peak during this period, showing that the anomalously high phytoplankton concentration was a result of intrinsic climate variability, and that the skillful prediction comes as a result of the initialization of NorCPM1 hindcasts. The positive chlorophyll anomaly seen in the reanalysis and the satellite data in the early 2010s is not predicted, which explains the overall low predictive skill in this region for the entire period of satellite observations displayed in Fig. 1. However, we note that the hindcasts follow the in situ observations that show a temporal evolution different from that in the satellite data, making it unclear whether there is any predictability during this later period of time.
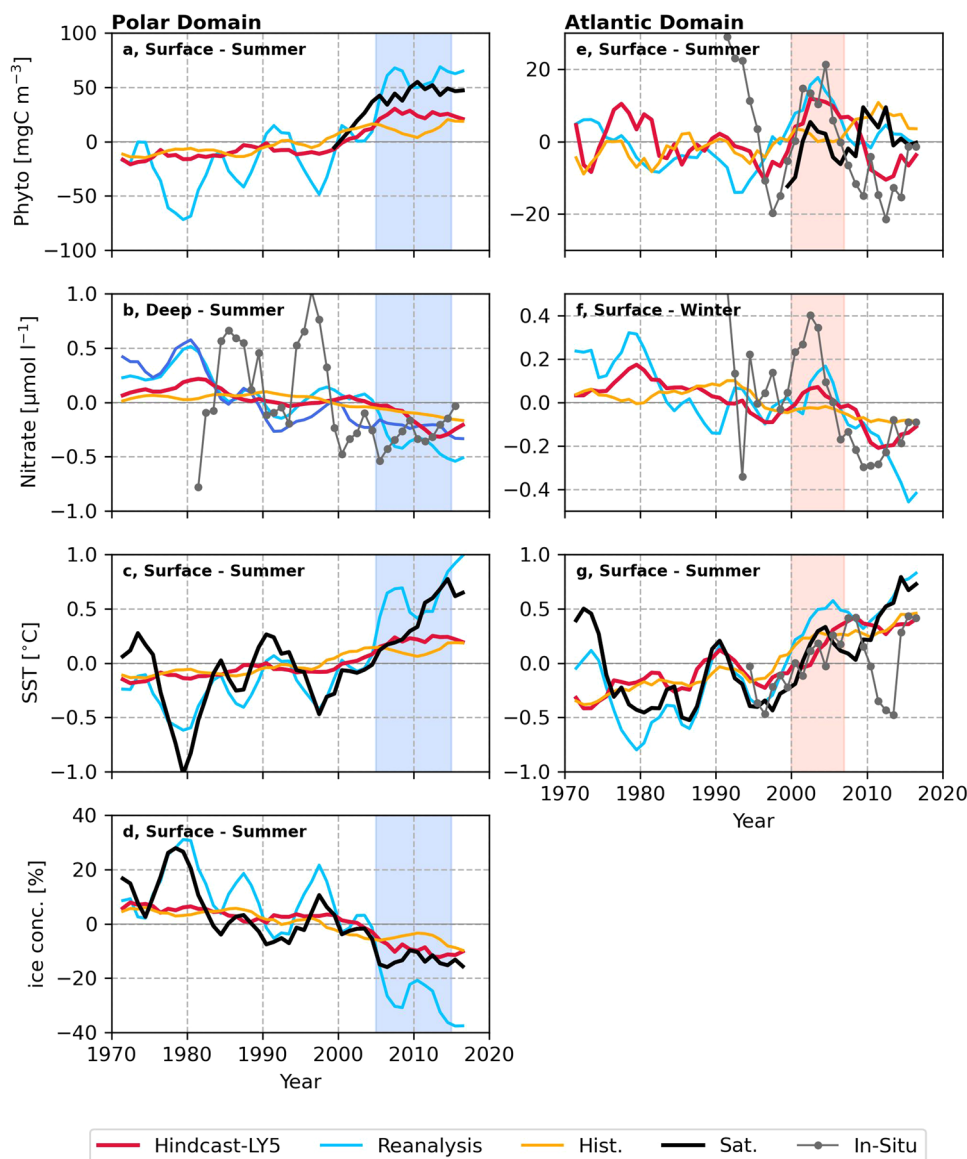
Fig. 2 Drivers of phytoplankton predictability. Anomaly time series of **a**, **e** phytoplankton concentration (mgC m^{-3}), **b**, **f** nitrate concentration (µmol l^{-1}), **c**, **g** sea surface temperature (°C), and **d** sea ice concentration (%) anomalies, from in situ measurements (gray line with points), satellite products (black), the historical simulation (orange), the reanalysis (blue) and the hindcasts at lead year 5 (red), in Polar Domain (left column) and Atlantic Domain (right column). The phytoplankton concentration, SST and ice concentration time series are the averages over May–July. For the nitrate time series in the Polar Domain, all available in situ data, mainly from the summer season, were used to construct the annual means, due to sparse sampling. These are compared to the summer (May–July) concentrations from the historical simulation, the reanalysis, and the hindcast. Here, the dark blue line shows the surface winter concentration for comparison. For the Atlantic Domain the winter nitrate concentrations (average over January–March) are shown. Note that all-time series have been filtered by a 4-year running mean. The shaded areas refer to time periods discussed in the text.

Similar to the Polar Domain, we analyze the time series of important drivers of primary production to understand what gave rise to the positive phytoplankton anomaly, and its predictability in the Atlantic Domain in the early 2000s (see also Supplementary Table S2). At lead year 5, the NorCPM1 hindcasts show positive anomalies in the winter concentrations of phosphate (Supplementary Fig. S3f) and nitrate (Fig. 2f) in the early 2000s. Increased concentrations of nutrients is partly confirmed by the available in situ data, where nitrate levels peaked in the early 2000s. In situ phosphate data, on the other hand, do not show such a peak (Supplementary Fig. S3f), but we do note that the magnitude of these variations are not far above the assumed uncertainty of these observations. The positive nutrient anomalies that co-occur with the positive phytoplankton anomaly, both in

the hindcasts and the observations, suggest that the prediction of the anomalously high phytoplankton is a result of the predictability of the nutrient levels at the start of the productive season. In addition, both the observational data and the hindcasts indicate an increased nutrient consumption in the period (Supplementary Fig. S5). Assuming a Redfield carbon:nitrogen ratio of 106:16 of the phytoplankton, the observed (modeled) nitrate drawdown of ~0.7(0.4) µmolN l^{-1} corresponds to an organic carbon concentration of 56(32) mgC m^{-3}, which is in good agreement with the observed (modeled) phytoplankton anomaly of 40(20) mgC m^{-3}. A lower organic carbon concentration in the phytoplankton biomass, compared to the converted nutrient drawdown, is expected due to grazing, exudation, and other loss processes. The good agreement between the nutrient

consumption anomaly and the phytoplankton concentration anomaly, in both observations and the hindcasts, confirms that prediction of the winter nutrient concentration gave rise to the skillful prediction of increased phytoplankton activity in the early 2000s. Considering that nitrate is more limiting than phosphate both in the observations and the model (see Supplementary Fig. S6), and the absence of a phosphate anomaly in the in situ record, nitrate is most likely the main driver of this positive phytoplankton anomaly.

Satellite observations and the reanalysis show also a peak in the summer sea surface temperature (Fig. 2g) during the early 2000s. The hindcasts at lead year 5 reproduce this a few years late, suggesting that it is not the main reason for the high phytoplankton concentrations in the hindcasts. Other key drivers for phytoplankton dynamics, including downwelling shortwave radiation, mixed layer depth, and stratification, showed little predictability (Supplementary Fig. S3e–h and Table S2).

Advective pathways from the Subpolar North Atlantic. What gave rise to the predictability of the low summer sea ice concentration in the Polar Domain between 2005 and 2014, and the positive nutrient anomaly in the Atlantic Domain in the early 2000s, respectively?

Yeager et al.[16] showed that the 2007 winter sea ice minimum was caused by an anomalously strong northward heat transport from the SPNA, and that it could be predicted 5 years in advance with their climate prediction model (CESM). Although it is not captured by our skill score in lead year 5 due to the higher frequency variability in the observational data (Supplementary Table S1), NorCPM1 does predict an anomalously low winter sea ice extent during 2005–2014 (Supplementary Fig. S7). This is the result of an anomalously low sea ice growth due to a high heat loss from the ocean (Supplementary Fig. S8a, b). It is interesting to note that the predictability of this thermal ocean-ice coupling only takes place in the winter season, and not in the summer season (Supplementary Fig. S8c, d), suggesting that the predictability of the summer sea ice extent is the result of a persistence of the winter sea ice anomaly that extends into the summer season. In agreement with ref. [16], the anomalously low sea ice extent and high oceanic heat loss predicted by NorCPM1 can be related to heat advection from the SPNA. Figure 3a–e show maps of the residual (hindcast minus historical) upper-ocean (50–200 m) temperature anomaly for lead years 1–5 for the hindcast initialized in 2001. We note a positive temperature anomaly that builds up in the SPNA (lead years 1–2), spills over into the Nordic Seas (lead years 2–3), and enters the Barents Sea (lead years 3–5). This positive temperature anomaly is also present in the in situ measurements of Atlantic Water temperature at the Svinøy section, in good agreement with the hindcasts at lead year 1, although the hindcasts do not capture the first temperature peak in 2002 that is present in the observational record (Fig. 3f). At the Gimsøy section, an observed positive heat anomaly, peaking in 2004, is also reproduced by the hindcasts at lead year 3, although with a slight delay. The in situ measurements and model simulations clearly demonstrate the advective nature of the temperature anomaly and suggest that the low summer sea ice cover during 2005–2014 was caused by an anomalous advection of heat from the SPNA, which is in line with several studies that have shown a strong link between the heat transport through the BSO and the Barents Sea sea ice cover, both in observations and in models[7–9,23,31].

What about the Atlantic Domain, where nutrient concentrations at the start of the productive season was the main driver of the positive phytoplankton anomaly in the early 2000s? Considering that the nitrate concentration in the BSO also is

predictable at a 5-year lead, advection from the SPNA is the most probable mechanism underlying this predictability. Figure 3j–n shows maps of the residual (hindcast minus historical) nitrate anomaly for lead years 1–5 for the hindcast starting in 1998. In 1999–2000 (lead years 1–2), a positive nitrate anomaly builds up in the easternmost SPNA. It spills into the eastern Nordic Seas and travels northward with the Atlantic Water along the Norwegian coast in 2001 and 2002 (lead years 3–4). In 2003, at the 5-year lead, it enters the Barents Sea. The advective nature of this positive nitrate anomaly is corroborated by the in situ measurements of Atlantic Water nitrate at the Svinøy and Gimsøy sections, where it is manifested as peaks in 2000 and 2001, respectively. The modeled time series at these stations confirms that the model predicts the nitrate anomaly at lead years 2 and 4, respectively. The peak in nitrate in the early 1990s seen in the in situ measurements at both Svinøy and Gimsøy sections might be related to issues in the measurements themselves; it is well known that the measurement of nutrients were plagued with biases up until recent decades[32]. Therefore we do not emphasize these early peaks.

It is interesting to note the temporal shift in the positive temperature and nitrate anomalies at the Svinøy and Gimsøy in Fig. 3f–i, i.e., they do not occur simultaneously. This could either be a result of air–sea heat fluxes modifying the temperature anomalies en-route to the Barents Sea, or it suggests that the temperature and nitrate anomalies are linked to separate water masses. A detailed analysis of ocean heat budget and the temperature (heat) anomalies along the Atlantic Water pathways in the Nordic and Barents Seas is not performed here, which would be needed to quantify the separate roles of remote (advection) versus local (air–sea heat exchange) forcing in generating the temperature anomaly. Previous studies have, however, shown that advection is the dominant contributor to the heat anomalies in the Atlantic Domain of the Nordic Seas, and that air–sea heat fluxes play a secondary role[33–35]. Furthermore, since the nitrate and temperature anomalies already are shifted in the SPNA and southern Nordic Seas (compare Fig. 3f–i, respectively), it rather points to the argument of different water masses. Earlier studies have related a reduction of nutrients in the Nordic Seas with a contraction of the North Atlantic Subpolar Gyre, leading to an intrusion of more subtropical, nutrient-poor, waters[36,37]. It is also well known that a contraction of the subpolar gyre leads to warmer waters entering the Nordic Seas[38,39]. The subpolar gyre index, a proxy for the strength of the subpolar gyre circulation, shows a positive anomaly peaking in 1999, and a negative anomaly with a low in 2001 (Fig. 2 in ref. [40]). This timing is broadly consistent with the positive nutrient anomaly detected south of Svinøy in 1999, and the positive temperature anomaly that we start following in 2002, respectively (Fig. 3), and can therefore explain the appearance of these anomalies.

For the Barents Sea, the results in Supplementary Figs. S2, S4, S7, S9–S13 and Tables S1, S2 show absence of predictive skill in some of the lead years preceding lead year 5 for several of the variables analyzed. This may be a result of the role the advection plays in the predictability, in combination with spatial variations in the ability of the assimilation scheme to synchronize the reanalysis with the observational data. Fig. 6e in ref. [25] shows that the synchronization in NorCPM1 performs better further upstream, in the SPNA, compared to the Nordic Seas, which could explain the higher predictive skill at longer lead years in the Barents Sea.

Conclusions

Our results show that two events of anomalously high phytoplankton abundance in the Barents Sea are predictable up to
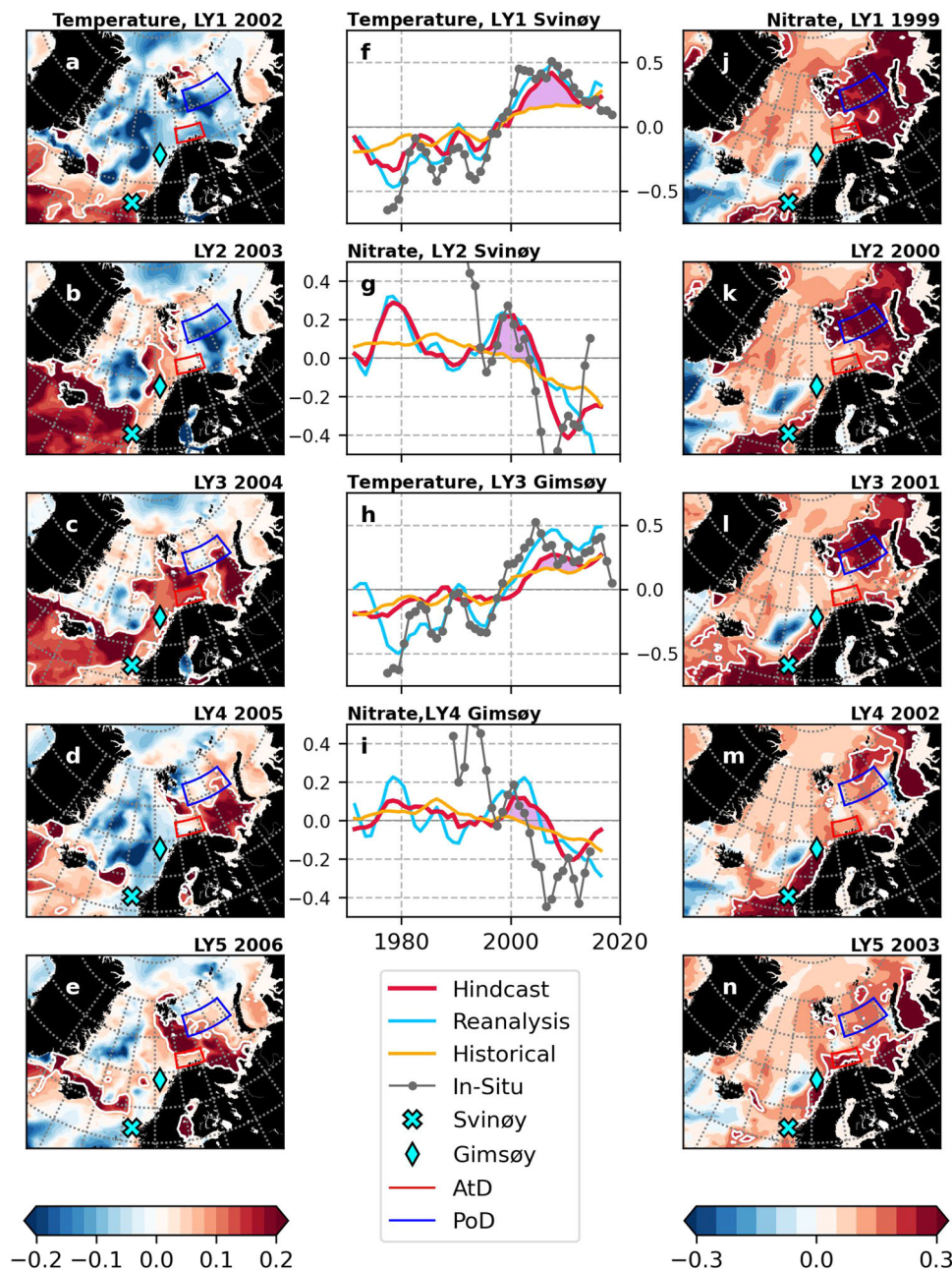
Fig. 3 Advective pathways. Maps showing the anomaly residual (hindcast minus historical) of 50–200 m annual mean temperature (°C) for lead years 1–5 (**a–e**) in the hindcast initialized in November 2001, and annual mean nitrate (μmol l⁻¹) for lead years 1–5 (**j–n**) for the hindcast initialized in November 1998. Time series of 50–200 m annual mean temperature and nitrate concentration, respectively, at the Svinøy (**f**, **g**) and Gimsøy (**h**, **i**) sections from in situ measurements (gray line with points), the historical simulation (orange), the reanalysis (blue) and the hindcasts at lead year 1 (**f**), 2 (**g**), 3(**h**), and lead year 4 (**i**) (red). Purple shading marks the respective hindcasted temperature and nitrate anomalies that are discussed in the text.

5 years in advance. This is, to our knowledge, among the longer predictability horizons reported for phytoplankton dynamics, based on retro-perspective hindcasts compared with observational data, in the global ocean[27,41,42]. We identify two different mechanisms giving rise to this predictability: in the ice-free Atlantic Domain it results from the advection of nutrient anomalies from the SPNA, while in the seasonally ice-covered Polar Domain it results from anomalous heat advection. We connect these anomalies to specific events of contraction and expansion, respectively, of the North Atlantic Subpolar Gyre. The mechanisms underlying the predictability are, therefore robust features that most likely will persist in the future. However, with the diminishing sea ice cover, the impact of the heat anomalies on

the Arctic Ocean primary productivity will likely become less important in the Barents Sea, but more important in the Arctic interior, where seasonal sea ice cover is quickly becoming the norm. Predictability of Barents Sea primary production may therefore be dominated by variability in the advection of nutrients from the SPNA, in the future.

Nevertheless, the multi-year predictability of the base of the marine food web in the Barents Sea demonstrated here adds confidence to the emerging number of studies[3,22,27,41–46] suggesting that near-time predictions of marine ecosystems may be feasible. Future research will need to investigate if, and how, this predictability can translate up to higher trophic levels in the Barents Sea.

Methods

Model simulations. We used simulations produced with the Norwegian Climate Prediction Model (NorCPM1[25]) for the sixth Coupled Model Intercomparison Project (CMIP6[47]) Decadal Climate Prediction Project (DCPP[48]). NorCPM1 is based on the Norwegian Earth System Model (NorESM1[26,49]) that has a global coverage, and includes the atmospheric model CAM4-OSLO with a 2-degree horizontal resolution, the ocean circulation model MICOM with a 1-degree horizontal resolution, the ocean biogeochemical model HAMOCC[26], the land model CLM4 and the sea ice model CICE4. HAMOCC simulates the dynamics of carbon, nitrogen, phosphorus, silicate and iron, and has one generic phytoplankton and one generic zooplankton group. Phytoplankton growth is constrained by the availability of light, nitrate, phosphate and dissolved iron, and the ambient temperature. The simulations used here include one extended historical simulation, one reanalysis, and one set of decadal retrospective predictions (hindcasts). The historical simulation was performed in 30 realizations (members) using CMIP6 historical forcing from 1850 to 2014, and was extended to 2029 by using SSP2-4.5 scenario forcing, in accordance with the DCPP protocol[25,48]. Each member was initialized by randomly selecting years (January months) from a preindustrial simulation, ensuring that they all had different climatic states (i.e., that they started from different oceanic and atmospheric states). A 30 member large reanalysis was performed for the period 1950 to 2018 with monthly assimilation of temperature and salinity anomalies using an Ensemble Kalman Filter[50,51], where ocean observations updates both the ocean and sea ice states (referred to as the assim-i2 simulation in ref. [25]). No assimilation of biogeochemical properties was performed[22]. Decadal hindcasts, consisting of 10 members each, were initialized on November 1st every year from the reanalysis (referred to as the hindcast-i2 simulations in ref. [25]). For further details on the simulation setup, the reader is referred to ref. [25].

Observational data. Satellite-derived chlorophyll concentration, used in sections "Prediction of phytoplankton abundance in NorCPM1" and "Local drivers of phytoplankton predictability", spanning 1998-present, were obtained from the OC-CCI dataset[52]. Satellite-derived sea ice concentration and SST, used in section "Local drivers of phytoplankton predictability", were obtained from the HadISST dataset[53](https://www.metoffice.gov.uk/hadobs/hadisst/). In situ measurements of macro-nutrients (nitrate and phosphate), used in the section "Local drivers of phytoplankton predictability", from the Barents and the Nordic seas from 1980–2017 are provided by the Norwegian Institute of Marine Research (IMR) and are available at http://www.imr.no/forskning/forskningsdata/infrastruktur/viewdataset.html?dataset_id=104 (last access: 28 June 2022). In situ measurements of temperature and salinity from CTD casts in the Barents Sea, used for the time series analysis in the sections "Local drivers of phytoplankton predictability", were obtained from the ICES data portal[54]. In the section "Advective pathways from the Subpolar North Atlantic", we additionally used preprocessed products of annual mean Atlantic Water (50–200 m depth) temperature and salinity from the hydrographic sections of Svinøy, Gimsøy, and Fugløya-Bjørnøya in the Barents Sea Opening, obtained from ICES (https://ocean.ices.dk/core/iroc[55]).

Data analysis and processing. We analyzed the predictability by evaluating the skill of the NorCPM1 hindcasts to predict observed temporal variations during the period where satellite data, in situ data, and model simulations are overlapping (1998–2018). To exclude variability on longer time scales than resolved by our time series, the time series were first linearly detrended. The prediction skill was then evaluated by (1) measuring the co-variability between detrended observed time series and the detrended simulated hindcasts through anomaly correlation and (2) thereafter by comparing their amplitude of variations through variances. If the correlation was significantly greater than zero, and if the variance of the hindcasted time series was of the same order of magnitude as the variance of the observed time series, we considered that the hindcasts skilfully predict the observations. The significance of the correlations was determined by calculating 95% confidence levels with a bootstrap approach, using 1000 bootstraps[22]. To identify the drivers of phytoplankton predictability we analyzed time series of key drivers of biological production, including temperature, sea ice cover, stratification, and the concentration of the macro-nutrients phosphate and nitrate, in surface and deep waters. To exclude that any predictive skill was caused by external forcing, such as anthropogenic greenhouse gases, aerosols, or volcanic eruptions, the skill was compared to that of the historical simulation, i.e., if an event that is present in the observed and hindcasted time series also exists in the historical simulation, it is considered to be a result of external forcing. To test the similarity between the hindcasted and historical time series we did two tests. If the correlation between the hindcasted and historical time series was significantly different from the correlation between the hindcasted time series and the observations, we considered that the predictive skill did not come from external forcing. If the correlations were not significantly different, we additionally compared the variance of the hindcasted and historical time series. If the variance of the historical simulation was one order of magnitude less than that of the hindcasted time series, we considered that the variability of the hindcasted time series was not a result of external forcing.

For the sake of clarity, we only present the ensemble means of the various simulations. For comparing model fields with satellite data, both products were regridded to 1×1-degree grids. For the comparison of the modeled phytoplankton abundance (expressed in carbon concentration) with the observed chlorophyll concentration, we used a C:Chl ratio of 120 to convert from mgChl m^{-3} to mgC m^{-3}, which is of the same order of magnitude as what has been observed in polar and subarctic waters[56,57]. We acknowledge that the C:Chl ratio can be highly variable[58]. However, with the few in situ measurements of this ratio that exist for the Barents Sea, we do not know how it varies on seasonal-to-interannual time scales, and thus, prefer to adopt the simpler approach. In the end, the exact choice of the C:Chl ratio will not significantly change the results presented since the analysis focus on interannual anomalies of phytoplankton abundance. We decided not to compare modeled primary production with satellite-derived primary production since the satellite NPP products contain several additional steps of data processing and, thus, larger uncertainties, compared to the satellite chlorophyll data.

A time series analysis was performed for two different regions within the Barents Sea; a northern Polar Domain located in the seasonally ice-covered region (74.5–77.5°N, 27.5–52.5°E, blue box in Fig. 1), and a southern Atlantic Domain located in ice-free waters (70.5–72.5°N, 19.5–32.5°E, red box in Fig. 1). Here, the data were divided into seasonal means for winter (January to March), and summer (May to July). We also performed a time series analysis of annual mean properties at two upstream hydrographic sections in the Nordic Seas. The procedure of extracting in situ data within the domains and at the sections depended on the data availability. For the Polar Domain, all available measurements within the blue box in Fig. 1 were extracted. For the Barents Sea Opening, in situ measurements from the Fugløya-Bjørnøya hydrographic section were extracted. Here, we removed all data north of 73°N and south of 72°N to minimize the influence of outflowing Polar Water and Norwegian Coastal Water, respectively[59]. To be comparable to satellite data, we use the uppermost layer (0–5 m) of the modeled fields for surface water properties. From the in situ measurements, which are generally sampled every 5 m, we use data from the uppermost 30 m for surface water properties. For deep water properties we restricted ourselves to the depth range of 50–200 m. In the section "Advective pathways from the Subpolar North Atlantic", we used preprocessed time series of annual mean Atlantic Water (defined as water in the depth range of 50–200 m) temperature at the hydrographic sections. These values have been calculated with data from three hydrographic stations centered around one single position, given as 63°N, 3°E for the Svinøy section, 69°N, 12°E for the Gimsøy section, and 73°N, 20°E for the Barents Sea Opening. To stay consistent with the temperature analysis, we extracted all observational data of nutrients within one degree of latitude and longitude from the same locations. Modeled temperature and nitrate concentration from the grid cell closest to these locations were extracted for the model-data comparison. To remove the year-to-year variability that is more influenced by chaotic atmospheric processes, and enhance the multi-year variability in which the more predictable oceanic processes reside, we applied a 4-year running mean on all-time series. To investigate the spatial coherence of the time series at the stations, maps of modeled residual anomalies of temperature and nitrate, averaged over 50–200 m, were produced. The residual anomalies were constructed by subtracting the historical simulation from the hindcasts. A similar methodology was used by ref. [60] to separate the internal variability from any externally forced variations. Note that for these maps, the time series were not subject to any running mean. All figures in the manuscript and the Supplementary Information were created with Python (https://www.python.org/). The arrow showing the pathway of the North Atlantic and Norwegian Atlantic currents in Fig. 1a) was created with Krita (https://krita.org/en/) and Inkscape (https://inkscape.org/).

Data availability

The CMIP6 DCPP NorCPM1 simulations[25,61–63] are available at the ESGF node: https://esgf-node.llnl.gov/search/cmip6/. Satellite-derived chlorophyll from the OC-CCI dataset[52,64] can be obtained at: https://climate.esa.int/en/projects/ocean-colour/data/ and ftp://oc-cci-data:ELaiWai8ae@oceancolour.org. HadISST data[53] were obtained from https://www.metoffice.gov.uk/hadobs/hadisst/ and are © British Crown Copyright, Met Office, 2020, provided under a Non-Commercial Government Licence http://www.nationalarchives.gov.uk/doc/non-commercial-government-licence/version/2/. In situ measurements of nutrients from the Barents and the Nordic seas[65] are available at http://www.imr.no/forskning/forskningsdata/infrastruktur/viewdataset.html?dataset_id=104 (last access: 28 June 2022). In situ measurements of temperature and salinity from CTD casts in the Barents Sea can be obtained from the ICES data portal[54]. Preprocessed products of annual mean Atlantic Water (50–200 m depth) temperature and salinity from the hydrographic sections of Svinøy, Gimsøy, and Fugløya-Bjørnøya in the Barents Sea Opening, were obtained from ICES (https://ocean.ices.dk/core/iroc[55]).

The SST data[66,67] used for Fig. 1a is found at https://data.ceda.ac.uk/neodc/esacci/sst/data/lt/Analysis/L4/v01.1/2007/04/15.

Code availability

The NorCPM1 model code can be obtained at GitHub (https://github.com/BjerknesCPU/NorCPM1-CMIP6). The Python scripts used to analyze the model and observational data can be obtained upon request to the authors.

References

1. Kjesbu, O. S. et al. Synergies between climate and management for atlantic cod fisheries at high latitudes. *Proc. Natl Acad Sci. USA* **111**, 3478–3483 (2014).
2. Bogstad, B., Dingsør, G. E., Ingvaldsen, R. B. & Gjøsæter, H. Changes in the relationship between sea temperature and recruitment of cod, haddock and herring in the barents sea. *Mar. Biol. Res.* **9**, 895–907 (2013).
3. Årthun, M. et al. Climate based multi-year predictions of the barents sea cod stock. *PLoS ONE* **13**, e0206319 (2018).
4. Dalpadado, P. et al. Climate effects on temporal and spatial dynamics of phytoplankton and zooplankton in the barents sea. *Progr. Oceanogr.* **185**, 102320 (2020).
5. Langehaug, H. R., Matei, D., Eldevik, T., Lohmann, K. & Gao, Y. On model differences and skill in predicting sea surface temperature in the nordic and barents seas. *Clim. Dyn.* **48**, 913–933 (2017).
6. Koul, V., Brune, S., Baehr, J. & Schrum, C. Impact of decadal trends in the surface climate of the north atlantic subpolar gyre on the marine environment of the barents sea. *Front. Mar. Sci.* https://www.frontiersin.org/articles/10.3389/fmars.2021.778335. (2022).
7. Årthun, M., Eldevik, T., Smedsrud, L. H., Skagseth, Ø. & Ingvaldsen, R. B. Quantifying the influence of atlantic heat on barents sea ice variability and retreat. *J. Clim.* **25**, 4736–4743 (2012).
8. Efstathiou, E., Eldevik, T., Årthun, M. & Lind, S. Spatial patterns, mechanisms, and predictability of barents sea ice change. *J. Clim.* **35**, 2961–2973 (2022).
9. Onarheim, I. H., Eldevik, T., Årthun, M., Ingvaldsen, R. B. & Smedsrud, L. H. Skillful prediction of barents sea ice cover. *Geophys. Res. Lett.* **42**, 5364–5371 (2015).
10. Wassmann, P. et al. Food webs and carbon flux in the barents sea. *Progr. Oceanogr.* **71**, 232–287 (2006).
11. Arrigo, K. R., van Dijken, G. & Pabi, S. Impact of a shrinking arctic ice cover on marine primary production. *Geophys. Res. Lett.* https://agupubs.onlinelibrary.wiley.com/doi/abs/10.1029/2008GL035028 (2008).
12. Oziel, L. et al. Role for atlantic inflows and sea ice loss on shifting phytoplankton blooms in the barents sea. *J. Geophys. Res. Oceans* **122**, 5121–5139 (2017).
13. Sandø, A. B. et al. Barents Sea plankton production and controlling factors in a fluctuating climate. *ICES J. Mar. Sci.* **78**, 1999–2016 (2021).
14. Helland-Hansen, B. & Nansen, F. *Report on Norwegian Fishery and Marine Investigations* Vol. 2 (Director of Fisheries, 1909).
15. Passos, L. et al. Impact of initialization methods on the predictive skill in norcpm: an arctic–atlantic case study. *Clim. Dyn.* https://doi.org/10.1007/s00382-022-06437-4 (2022).
16. Yeager, S. G., Karspeck, A. R. & Danabasoglu, G. Predicted slowdown in the rate of atlantic sea ice loss. *Geophys. Res. Lett.* **42**, 10704–10713 (2015).
17. Koul, V. et al. Skilful prediction of cod stocks in the north and barents sea a decade in advance. *Commun. Earth Environ.* **2**, 140 (2021).
18. Germe, A., Chevallier, M., Salas y Mélia, D., Sanchez-Gomez, E. & Cassou, C. Interannual predictability of arctic sea ice in a global climate model: regional contrasts and temporal evolution. *Clim. Dyn.* **43**, 2519–2538 (2014).
19. Guemas, V. et al. A review on arctic sea-ice predictability and prediction on seasonal to decadal time-scales. *Q. J. R. Meteorol. Soc.* **142**, 546–561 (2016).
20. Bushuk, M. et al. Skillful regional prediction of arctic sea ice on seasonal timescales. *Geophys. Res. Lett.* **44**, 4953–4964 (2017).
21. Kimmritz, M. et al. Impact of ocean and sea ice initialisation on seasonal prediction skill in the arctic. *J. Adv. Model. Earth Syst.* **11**, 4147–4166 (2019).
22. Fransner, F. et al. Ocean biogeochemical predictions–initialization and limits of predictability. *Front. Mar. Sci.* https://www.frontiersin.org/articles/10.3389/fmars.2020.00386 (2020).
23. Dai, P. et al. Seasonal to decadal predictions of regional arctic sea ice by assimilating sea surface temperature in the Norwegian climate prediction model. *Clim. Dyn.* **54**, 3863–3878 (2020).
24. Shi, H. et al. Global decline in ocean memory over the 21st century. *Sci. Adv.* **8**, eabm3468 (2022).
25. Bethke, I. et al. Norcpm1 and its contribution to cmip6 dcpp. *Geosci. Model Dev.* **14**, 7073–7116 (2021).
26. Tjiputra, J. F. et al. Evaluation of the carbon cycle components in the norwegian earth system model (noresm). *Geosci. Model Dev.* **6**, 301–325 (2013).
27. Séférian, R. et al. Multiyear predictability of tropical marine productivity. *Proc. Natl Acad. Sci. USA* **111**, 11646–11651 (2014).
28. Arrigo, K. R. & van Dijken, G. L. Secular trends in arctic ocean net primary production. *J. Geophys. Res. Oceans* https://agupubs.onlinelibrary.wiley.com/doi/abs/10.1029/2011JC007151 (2011).
29. Arrigo, K. R. & van Dijken, G. L. Continued increases in arctic ocean primary production. *Progr. Oceanogr.* **136**, 60–70 (2015).
30. Olsen, A. et al. The global ocean data analysis project version 2 (glodapv2) – an internally consistent data product for the world ocean. *Earth Syst. Sci. Data* **8**, 297–323 (2016).
31. Sandø, A. B., Nilsen, J. E. Ø., Gao, Y. & Lohmann, K. Importance of heat transport and local air-sea heat fluxes for barents sea climate variability. *J. Geophys. Res. Oceans* https://agupubs.onlinelibrary.wiley.com/doi/abs/10.1029/2009JC005884 (2010).
32. Olsen, A. et al. An updated version of the global interior ocean biogeochemical data product, glodapv2.2020. *Earth Syst. Sci. Data* **12**, 3653–3678 (2020).
33. Carton, J. A., Chepurin, G. A., Reagan, J. & Häkkinen, S. Interannual to decadal variability of atlantic water in the nordic and adjacent seas. *J. Geophys. Res. Oceans* https://agupubs.onlinelibrary.wiley.com/doi/abs/10.1029/2011JC007102 (2011)
34. Asbjørnsen, H., Årthun, M., Skagseth, Ø. & Eldevik, T. Mechanisms of ocean heat anomalies in the norwegian sea. *J. Geophys. Res. Oceans* **124**, 2908–2923 (2019).
35. Asbjørnsen, H., Årthun, M., Skagseth, Ø. & Eldevik, T. Mechanisms underlying recent arctic atlantification. *Geophys. Res. Lett.* **47**, e2020GL088036 (2020).
36. Rey, F. Declining silicate concentrations in the Norwegian and Barents Seas. *ICES J. Mar. Sci.* **69**, 208–212 (2012).
37. Hátún, H. et al. The subpolar gyre regulates silicate concentrations in the north atlantic. *Sci. Rep.* **7**, 14576 (2017).
38. Hátún, H., Sandø, A. B., Drange, H., Hansen, B. & Valdimarsson, H. Influence of the atlantic subpolar gyre on the thermohaline circulation. *Science* **309**, 1841–1844 (2005).
39. Asbjørnsen, H., Johnson, H. L. & Årthun, M. Variable nordic seas inflow linked to shifts in north atlantic circulation. *J. Clim.* **34**, 7057–7071 (2021).
40. Hátún, H. & Chafik, L. On the recent ambiguity of the north atlantic subpolar gyre index. *J. Geophys. Res. Oceans* **123**, 5072–5076 (2018).
41. Park, J.-Y., Stock, C. A., Dunne, J. P., Yang, X. & Rosati, A. Seasonal to multiannual marine ecosystem prediction with a global earth system model. *Science* **365**, 284–288 (2019).
42. Brune, S. et al. Oceanic rossby waves drive inter-annual predictability of net primary production in the central tropical pacific. *Environ. Res. Lett.* **17**, 014030 (2022).
43. Chikamoto, M. O., Timmermann, A., Chikamoto, Y., Tokinaga, H. & Harada, N. Mechanisms and predictability of multiyear ecosystem variability in the north pacific. *Global Biogeochem. Cycles* **29**, 2001–2019 (2015).
44. Frölicher, T. L., Ramseyer, L., Raible, C. C., Rodgers, K. B. & Dunne, J. Potential predictability of marine ecosystem drivers. *Biogeosciences* **17**, 2061–2083 (2020).
45. Krumhardt, K. M. et al. Potential predictability of net primary production in the ocean. *Global Biogeochem. Cycles* **34**, e2020GB006531 (2020).
46. Payne, M. R. et al. Skilful decadal-scale prediction of fish habitat and distribution shifts. *Nat. Commun.* **13**, 2660 (2022).
47. Eyring, V. et al. Overview of the coupled model intercomparison project phase 6 (cmip6) experimental design and organization. *Geosci. Model Dev.* **9**, 1937–1958 (2016).
48. Boer, G. J. et al. The decadal climate prediction project (dcpp) contribution to cmip6. *Geosci. Model Dev.* **9**, 3751–3777 (2016).
49. Bentsen, M. et al. The norwegian earth system model, noresm1-m – part 1: description and basic evaluation of the physical climate. *Geosci. Model Dev.* **6**, 687–720 (2013).
50. Counillon, F. et al. Seasonal-to-decadal predictions with the ensemble kalman filter and the Norwegian earth system model: a twin experiment. *Tellus A: Dyn. Meteorol. Oceanogr.* **66**, 21074 (2014).
51. Counillon, F. et al. Flow-dependent assimilation of sea surface temperature in isopycnal coordinates with the norwegian climate prediction model. *Tellus A: Dyn. Meteorol. Oceanogr.* **68**, 32437 (2016).
52. Sathyendranath, S. et al. An ocean-colour time series for use in climate studies: the experience of the ocean-colour climate change initiative (oc-cci). *Sensors* https://www.mdpi.com/1424-8220/19/19/4285 (2019).
53. Rayner, N. A. et al. Global analyses of sea surface temperature, sea ice, and night marine air temperature since the late nineteenth century. *J. Geophys. Res. Atmos.* https://agupubs.onlinelibrary.wiley.com/doi/abs/10.1029/2002JD002670 (2003).
54. ICES data portal, dataset on ocean hydrochemistry. https://data.ices.dk/ International Council for the Exploration of the Sea (ICES), Copehagen. (2022).
55. Gonzalez-Pola, C., Larsen, K. M. H., Fratantoni, P. & Beszczynska-Möller, A. ICES Report on ocean climate 2020. ICES Cooperative Research Reports (CRR). Report. https://doi.org/10.17895/ices.pub.19248602.v2. Data access: https://ocean.ices.dk/core/iroc (2022).

56. Verity, P. G., Smayda, T. J. & Sakshaug, E. Photosynthesis, excretion, and growth rates of phaeocystis colonies and solitary cells. *Polar Res.* **10**, 117–128 (1991).

57. Hansen, B., Christiansen, S. & Pedersen, G. Plankton dynamics in the marginal ice zone of the central barents sea during spring: carbon flow and structure of the grazer food chain. *Polar Biol.* **16**, 115–128 (1996).

58. Behrenfeld, M. J. et al. Revaluating ocean warming impacts on global phytoplankton. *Nat. Clim. Change* **6**, 323–330 (2016).

59. Olsen, A., Johannessen, T. & Rey, F. On the nature of the factors that control spring bloom development at the entrance to the barents sea and their interannual variability. *Sarsia* **88**, 379–393 (2003).

60. Smith, D. M. et al. Robust skill of decadal climate predictions. *npj Clim. Atmos. Sci.* **2**, 13 (2019).

61. Bethke, I. et al. NCC NorCPM1 model output prepared for cmip6 cmip historical-ext. https://doi.org/10.22033/ESGF/CMIP6.10895 (2020).

62. Bethke, I. et al. NCC NorCPM1 model output prepared for cmip6 dcpp dcppa-assim. https://doi.org/10.22033/ESGF/CMIP6.10864 (2019).

63. Bethke, I. et al. NCC NorCPM1 model output prepared for cmip6 DCPP dcppa-hindcast. https://doi.org/10.22033/ESGF/CMIP6.10865 (2019).

64. Sathyendranath, S. et al. Esa ocean colour climate change initiative (ocean_colour_cci): Version 5.0 data. https://climate.esa.int/en/projects/ocean-colour/data/ (2021).

65. Institute of Marine Research. Næringssalt-, oksygen- og klorofyll- data i norske havområder fra 1980–2017. http://www.imr.no/forskning/forskningsdata/infrastruktur/viewdataset.html?dataset_id=104 (2022).

66. Merchant, C. et al. Esa sea surface temperature climate change initiative (ESA SST CCI): analysis long term product version 1.1. https://data.ices.dk/ (2016).

67. Merchant, C. J. et al. Satellite-based time-series of sea-surface temperature since 1981 for climate applications. *Sci. Data* **6**, 223 (2019).

68. Good, S., Embury, O., Bulgin, C. & Mittaz, J. Esa sea surface temperature climate change initiative (sst_cci): level 4 analysis climate data record, version 2.1. *Centre Environ. Data Anal.* https://doi.org/10.5285/62c0f97b1eac4e0197a674870afe1ee6. (2019).

Acknowledgements

Author contributions

F.F. performed the data analysis. All authors participated in the discussion of the results and in the design of the data analysis. F.F. lead the writing with contributions from A.O, M.Å., F.C., J.T., A.S., and N.K.

Funding

Competing interests

The authors declare no competing interests.

Additional information

Supplementary information The online version contains supplementary material available at https://doi.org/10.1038/s43247-023-00791-9.

Correspondence and requests for materials should be addressed to Filippa Fransner.

Peer review information *Communications Earth & Environment* thanks Laurent Oziel and the other, anonymous, reviewer(s) for their contribution to the peer review of this work. Primary Handling Editors: Ilka Peeken and Clare Davis. Peer reviewer reports are available.

Reprints and permission information is available at http://www.nature.com/reprints

Publisher's note Springer Nature remains neutral with regard to jurisdictional claims in published maps and institutional affiliations.